NANO LETTERS

pubs.acs.org/NanoLett Letter

Crystallization-Induced Shift in a Triboelectric Series and Even Polarity Reversal for Elastic Triboelectric Materials

Zhaoqi Liu, Shuyao Li, Shiquan Lin, Yuxiang Shi, Peng Yang, Xiangyu Chen,* and Zhong Lin Wang*

Cite This: https://doi.org/10.1021/acs.nanolett.2c00767 Read Online

ACCESS | Metrics & More | Article Recommendations | Supporting Information

ABSTRACT: A stretchable triboelectric nanogenerator (TENG) can be a promising solution for the power supply of various flexible electronics. However, the detailed electrification mechanism of elastic triboelectric materials still needs to be clarified. In this work, we found crystallization behavior induced by strain and low temperature can lead to a shift in a triboelectric series for commonly used triboelectric elastomers and even reverse the triboelectric polarity. This effect is attributed to the notable rearrangement of surface electron cloud density happening along with the crystallization process of the molecular chain. This effect is significant with natural rubber, and silicone rubber can experience this effect at low temperature, which also leads to a shift in a triboelectric series, and an applied strain at low temperature can further enhance this shift. This study demonstrated that the electrification polarity of triboelectric materials should be re-evaluated under different strains and different temperatures, which provides a mechanism distinct from the general understanding of elastic triboelectric materials.

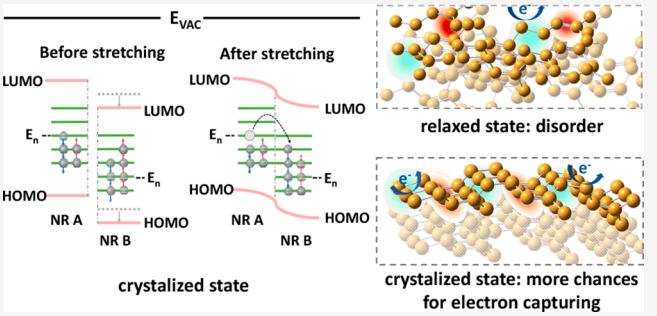

KEYWORDS: *triboelectric nanogenerator, elastomer, electrification mechanism, triboelectric series*

Flexible and stretchable electronics have drawn a great deal of attention in today's technological world, where the mechanical compliance and biocompatibility of the electronic devices is the focus of the research.[1−3] In addition to the electronic devices, the power units, such the batteries and energy-harvesting packages, are also required to be flexible and even highly stretchable,[4] in order to support portable and wearable electronic systems. In this application direction, triboelectric nanogenerators (TENGs), which have a strong adaptability,[5,6] high flexibility,[7] and good environmental friendliness,[8] have been applied to power various soft electronic and sensory systems to achieve diversified functions.[9−11] In the past few years, tremendous efforts have been devoted to amplify the stretchability of TENGs by adopting a series of elastic electrification materials, such as deformable networks (200−300%),[12] silicone and rubber (400−700%),[13,14] an ionic hydrogel (1000%),[15−17] and a thermoplastic elastomer (~2500%).[18] However, even though extensive progress have been achieved in the exploration of stretchable TENGs and superelastic triboelectric materials,[19,20] an in-depth study of the strain-induced change in the electrification capability of triboelectric materials is seemingly absent.

Most stretchable TENGs utilize polymer materials, such as all kinds of elastomers.[21−23] Meanwhile, many studies have revealed that the characteristics and the density of functional groups in a polymer can determine the electron transfer process during contact electrification.[24−28] For the commonly used stretchable triboelectric materials, the applied strain can induce many changes in the electrification process, while the underlying mechanism remains ambiguous. Usually, a change in the effective contact area[29,30] and the induced intermolecular forces[31,32] is considered to be the major effect changing the electrification performance. During the stretching, the applied stress may change the composition of functional groups exposed on the polymer surface, while the stretching-induced crystallization of soft segments may also occur with some materials.[33−35] Hence, a systematic study of the influences of strain-induced crystallization (SIC) on the contact electrification is also quite necessary to promote the development of stretchable and wearable TENGs.

In this paper, we have found that a crystallization effect occurring on a elastic polymer can shift its ranking in the triboelectric series and, accordingly, the related TENG devices may have different electrification polarities under different strains or at different temperatures. On the basis of an analysis of the molecular structure, this strain-induced shift of the triboelectric series happens when ordered and large-scale

Received: February 24, 2022
Revised: May 3, 2022

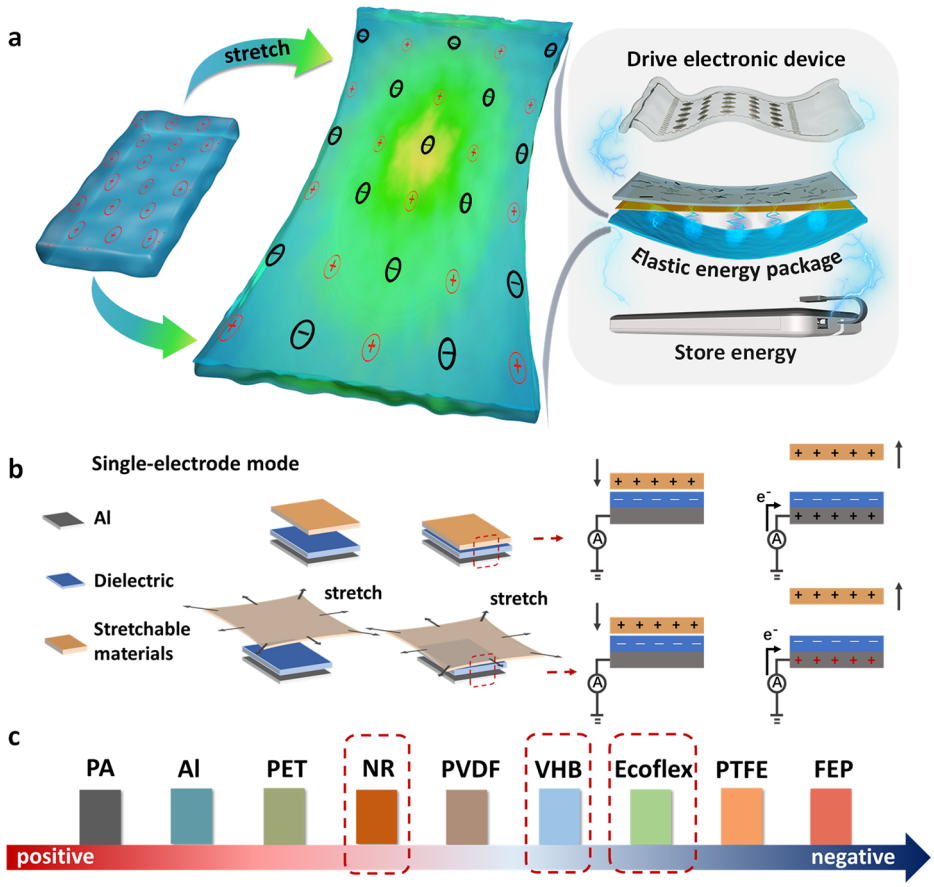

Figure 1. (a) Application of elastic materials in a stretchable TENG, which promotes the applications of an energy package and active sensors. (b) Schematic diagram of the measurement method in experiments with stretchable triboelectric materials. (c) Ranking of VHB, Ecoflex, and NR in a triboelectric series.

changes in the molecular orientation appears, where the rearrangement of the electron cloud density on the surface is the key point. This study reveals the correlation between electrification performance and a strain (or temperature)-induced change at the molecular level, which helps us to better understand the contribution of the molecular spatial orientation of a polymer to its macroscopic electrical properties.

The emergence of stretchable TENGs have strongly promoted the development of flexible electronic devices, where an elastic energy package based on a TENG can realize the function of a power supply, energy storage,[36] or even self-powered sensors for wearable electronic devices[37,38] (see Figure 1a). As can be seen in Figure 1b, we selected a single-electrode mode[39] TENG with vertical contact-separation motion for the experiments, where the thickness of the elastomer may have a very limited effect on the output results in this case. The experimental system and working principle of a TENG is also shown in Figure 1b and Note 1 in the Supporting Information. Three representative stretchable materials commonly used in flexible TENG have been selected, and to the best of our nowledge, most of the previously reported stretchable TENGs contain these three materials or their composites.[40−42] They are silicon rubber (Ecoflex 00-30), a polyacrylate elastomer (VHB-4905) ,and unsaturated rubber (NR) (photos of these three polymers are shown in Figure S1), which represent three typical types of elastic triboelectric materials: a pure elastomer, a copolymer, and an impure elastomer (the intrinsic triboelectric series of these materials[43] is given in Figure 1c).

The saturated charge density (absolute value) on the contact interface is shown in Figure 2a. Here, the surface potential of the initial state was confirmed by a Trek 347 instrument after treatment (Figure S2). For the measurement, each sample is tested at least 10 times to avoid measurement errors during the test. Through measurement, it is found that the three kinds of elastomers show completely different change tendencies in the tensile process. In the process of contacting with FEP, the charge density of NR (100%, relaxed state; 26 μC m^{-2}) decreases greatly with an increase in applied strain, when it is stretched to 400%, the saturated charge density decreases to 14 μC m^{-2}. In contrast, the experimental results are quite different when NR is contacted with PA (positive material). At the initial state, the saturated charge density between NR and a PA film is around 19 μC m^{-2}. With an applied strain, the CE charge density of NR (400%) increases to 23.5 μC m^{-2} (Figure S3). The result of this distinct change tendency with FEP and PA suggests that NR has a ranking shift in the triboelectric series under applied strains. A similar effect cannot be observed with Ecoflex and VHB films. As can also be seen in Figure 2a, the saturated charge density of Ecoflex decreases from 23 μC m^{-2} (100%) to 19.5 μC m^{-2} (400%) when it is coupled with FEP film, which makes it rather stable in comparison with the other two materials. When Ecoflex is contacted with a PA film, its saturated charge density decreases from 37 to 34 μC m^{-2} and the change ratio of which is even smaller. A similar change

https://doi.org/10.1021/acs.nanolett.2c00767
Nano Lett. XXXX, XXX, XXX−XXX

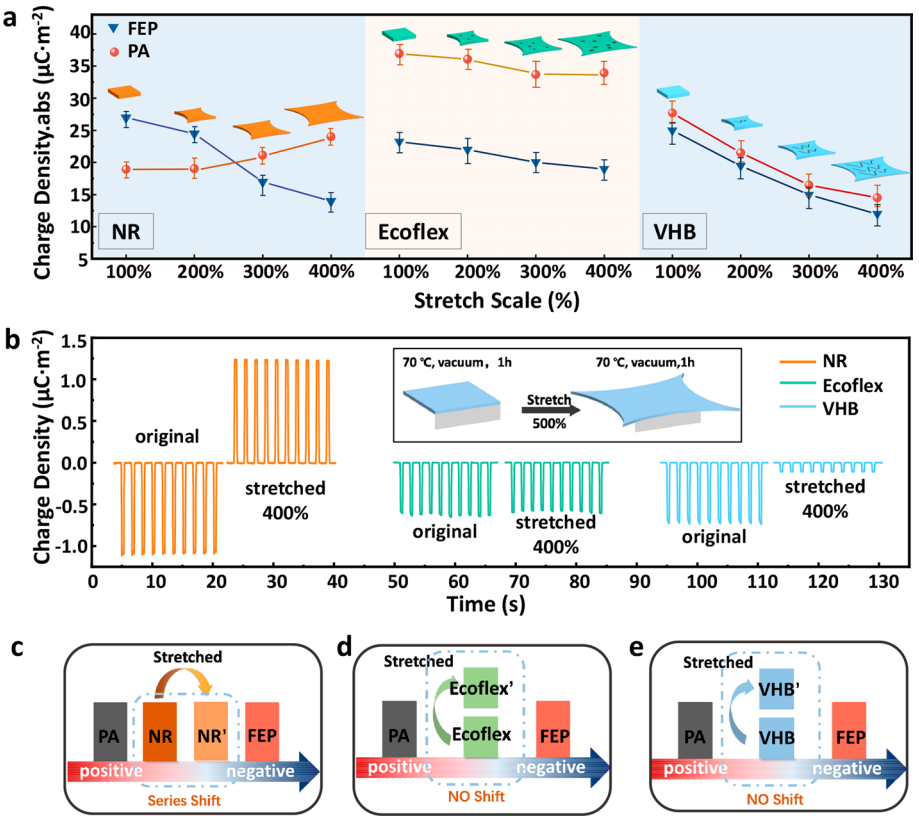

Figure 2. (a) Saturated charge densities (absolute value) of NR, Ecoflex, and VHB with FEP (negative) and PA (positive), respectively. The density changes before and after stretching are also recorded. (b) Saturated charge densities of NR, Ecoflex, and VHB contacted with themselves before and after stretching. A turnover effect happens with NR. Changes in ranking of VHB, Ecoflex, and NR in a triboelectric series: (c) NR film; (d) Ecoflex film; (e) VHB film.

tendency has also been observed with VHB film. The saturated charge density of VHB in contact with FEP also decreased from 25 μC m^{-2} (100%) to 15 μC m^{-2} (400%), while the density coupled with PA decreased from 28 μC m^{-2} before stretching to 14 μC m^{-2} with 400% strain. We have further studied the turnover phenomenon of the polarity by using these elastic films, as can be seen in Figure 2b,c, Figure S4 and Movie 1. A detailed description can be found in Note 1 in the Supporting Information.

The characterization of surface morphology is the first step in explaining the electrification results in Figure 2. The morphological changes of the three materials after stretching were observed by a high-power optical microscope. It can be seen from Figure 3a–d and Figure S5 that the surface morphologies of both NR and Ecoflex shows a slight change even when the tensile ratio is 600%. Moreover, an atomic force microscope (AFM) with higher resolution was used to recheck the surface roughness of three materials before and after stretching, and the results are shown in Figure S6 and Table S1. Here, the results from AFM measurements are in good agreement with the observations from an optical microscope. All three materials become rougher after stretching, which is due to the wrinkles induced during the stretching process, and the change in roughness has a similar tendency and similar amplitude. However, the distinct phenomenon occurred only on NR, which supports our consideration of a crystallization effect. Hence, the surface morphology is not the dominating factor in the shift in the triboelectric series, especially considering that the soft texture of all these materials may suppress the influences caused by the tiny changes in roughness. Meanwhile, some small holes appeared on the surface of Ecoflex after stretching, while the change ratio of the effective area is still less than 10%. A similar effect happens more significantly with VHB film, where a series of wrinkles can be observed (see Figure 3e,f). As explained in Materials and Method in the Supporting Information, UV pretreatment is applied on the VHB surface, in order to reduce the viscosity. When VHB is stretched to 600%, the holes on the surface are torn into cracks, and 80% of the surface becomes cavities. These cavities are considered to be the main factor for the decrease in the electrification capacity of this elastic material (VHB). Other elastic materials similar to the UV-treated VHB whose surfaces are easy to crack after stretching may have similar effects during CE, which directly leads to a decrease in the saturated charge density. In order to study the homogeneity of the surface potential, the surface potential of an NR film before and after stretching was measured by a Trek 347 electrostatic voltmeter. The 3D potential diagram of the original electrostatic potential of an NR surface contacted with FEP is shown in Figure 3g. Then, the film was stretched to 400% and the electrostatic potential is shown in Figure 3h. The average potential after stretching (42.70 V) is lower than that before stretching (81.2 V), while the homogeneities of the surface potential are almost the same.

On the basis of previous studies of thermal emission and photoexcitation,[6,44,45] we prefer the viewpoint of electron transfer to explain the experimental results in this work. The changes in functional groups of three films after stretching have been analyzed by attenuated total reflection-Fourier transform infrared (ATR-FTIR) spectroscopy. As shown in Figure S7,

https://doi.org/10.1021/acs.nanolett.2c00767
Nano Lett. XXXX, XXX, XXX−XXX

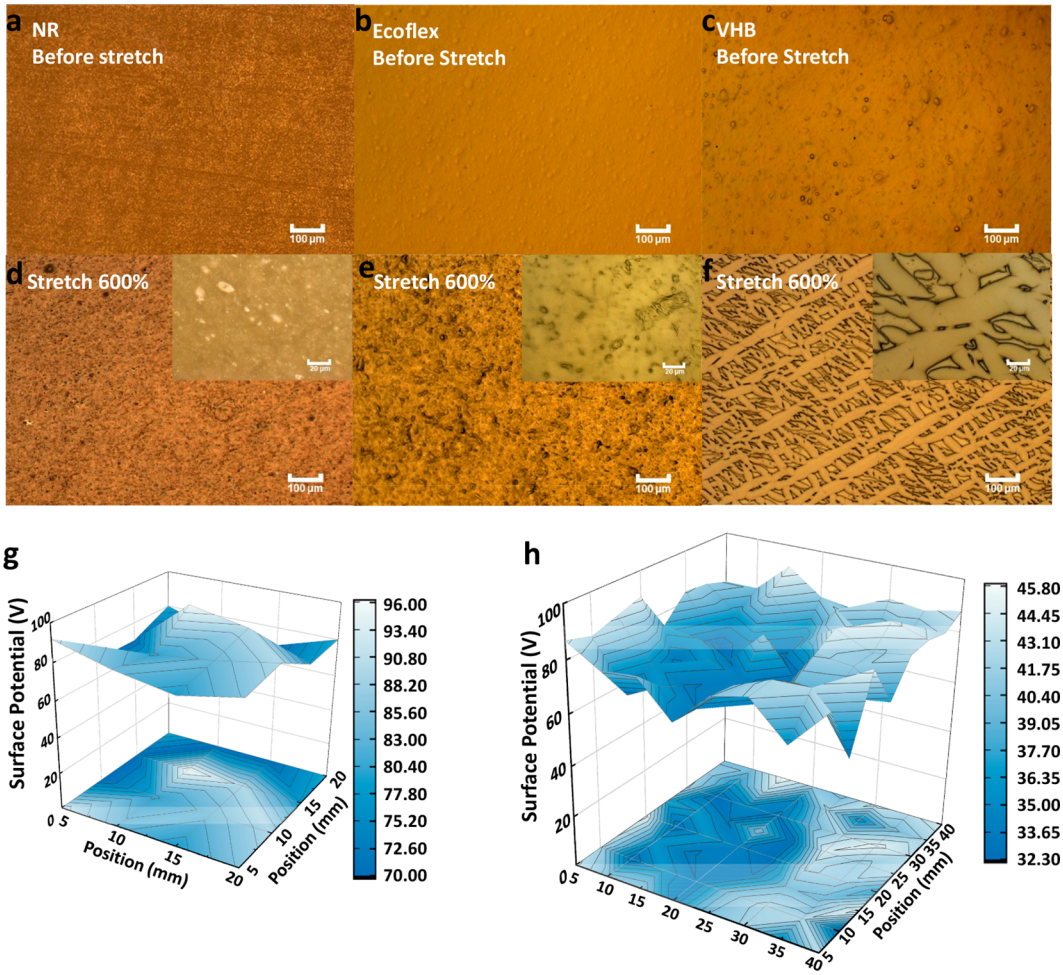

Figure 3. Changes in the surface morphology of stretchable materials during stretching (600%) as observed by an optical microscope: (a) NR before stretching; (b) Ecoflex before stretching; (c) VHB before stretching; (d), NR after stretching 600%; (e) Ecoflex after stretching 600%; (f), VHB after stretch ing600%. (g, h) Electrostatic potentials of the NR surface before and after stretching (400%) measured by a Trek 347 instrument.

the infrared spectra of VHB and Ecoflex show little change after stretching, suggesting that there is no rearrangement of functional groups caused by the change in spatial structure. On the basis of the Wang transition model[46] for electrification, the electron-withdrawing ability and density of functional groups on the main chain can change the electron density on the surface region, which leads to a change in polarity and strength of the CE effect. Hence, ATR-FTIR results further proved that the changes in the electrification capacities of VHB and Ecoflex under strain are mainly caused by a decrease in effective contact area during the morphology change. The changes in structures of NR are given by a Fourier transform infrared (ATR-FTIR) spectrum (see Figure 4a), the orientation of NR after stretching has been analyzed by polarized ATR-FTIR spectroscopy (see Figure 4b), and the crystal structures of NR before and after stretching have been measured by X-ray diffraction (XRD), as shown in Figure S8. For crystalline and oriented polymers, the molecular chain has a certain orientation; thus, the incident polarized infrared light in the sample leads to different absorption intensities. The result in Figure 4b shows that the parallel and vertical absorption bands of NR do not completely coincide. The orientation function of NR after stretching has been calculated (see Figure S9), which confirms that the orientation and SIC of NR are produced under strain in the experiment. More than 95% of the main component of NR is *cis*-1,4-polyisoprene, while it also contains some impurities such as protein and fatty acids. In Figure 4a, it can be seen that the vibration intensity of the amide (−CONH−) group at 1540 cm^{-1} decreases significantly after stretching. This functional group, whose amount decreases after stretching, acts as an electron-donor group, resulting in the suppression of the electron-donating capability of NR after stretching. The peak at 835 cm^{-1} is identified as the C−H out-of-plane bending, which is considered to be related to the *cis* structure of *cis*-1,4-polyisoprene.[47,48] The strength of this peak increases greatly under strain, and the ranking moved to the high-wavenumber direction (835 cm^{-1} moves to 840 cm^{-1} when NR is stretched to 400%). This absorption band at 840 cm^{-1} was considered to be specific to crystalline regions in previous studies.[49,50] The shift of the peak proves that the conformation of *cis*-1,4-polyisoprene has changed. In order to study the potential distribution of functional groups in the whole molecule, the chain elements were calculated by density functional theory (DFT). The electrostatic potential diagram of the chain elements is shown in Figure 4c, in which the blue and red areas are positive and negative potential areas, corresponding to electron-poor areas and electron-rich areas, respectively. Therefore, C═C provides an electron donor conjugation effect in the polyisoprene molecule. It can also be seen from a molecular orbital simulation diagram (Figure S10)

https://doi.org/10.1021/acs.nanolett.2c00767
Nano Lett. XXXX, XXX, XXX−XXX

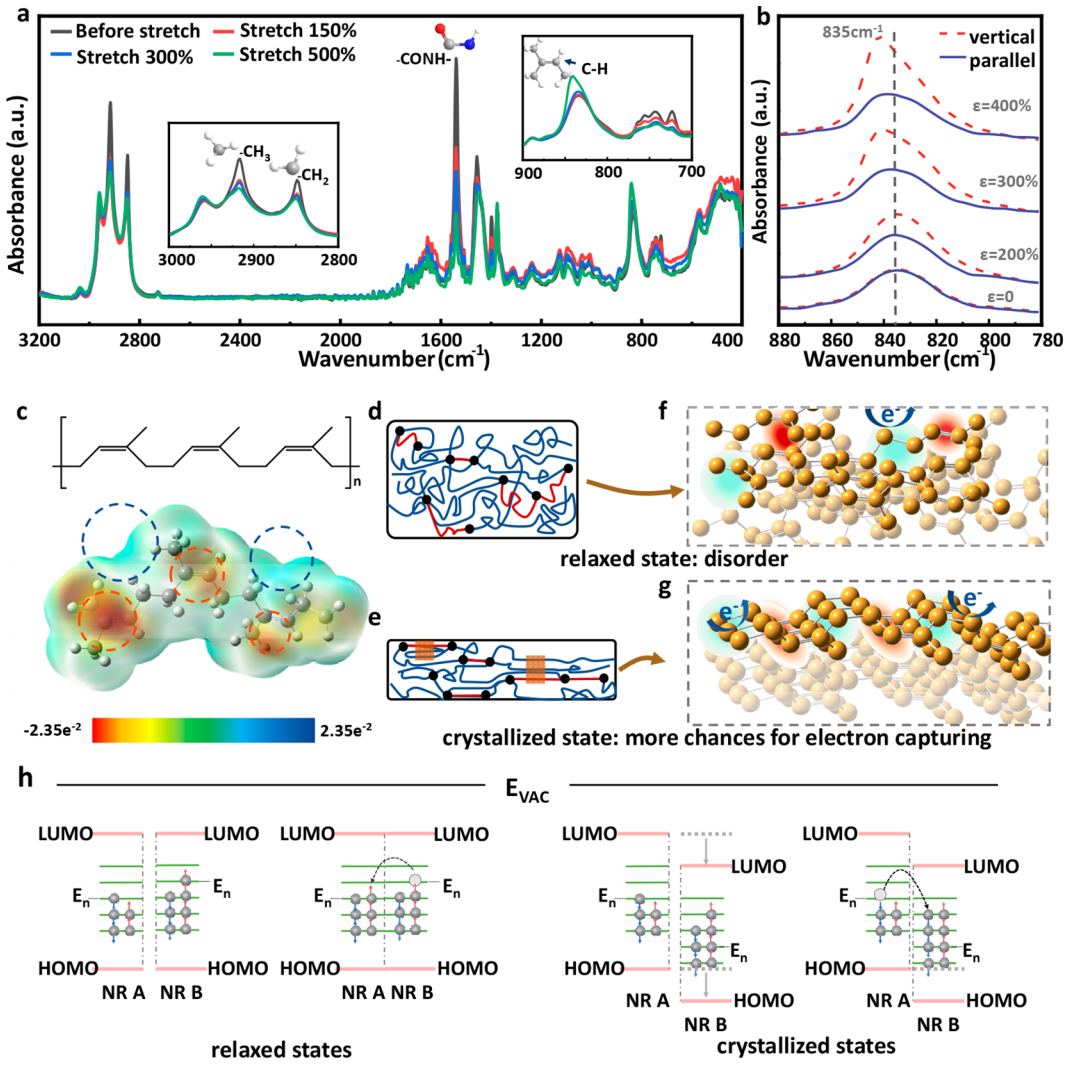

Figure 4. (a) Structures of NR at different stretching scales as given by a Fourier transform infrared (ATR-FTIR) spectrum. (b) Polarized infrared spectrum showing the change of the peak at 835 cm^{-1} of NR. (c) Electrostatic potential map of *cis*-1,4-polyisoprene (chain element of NR). (d–g) Schematic models illustrating the corresponding structures of the NR before and after stretching. (h) Theoretical diagram to explain the charge transfer between NR before and after stretching. Definitions: E_{VAC}, vacuum level of surface states; E_n, neutral level of surface states.

that the electron cloud orbital corresponding to C═C is larger than that corresponding to C−H. Hence, the crystallization of NR makes the molecular chain more orderly, which results in exposing an electron-poor area (C−H) to the surface side and hiding the electron-donating bond (C═C) to the bulk region and increasing the total electron-withdrawing capability of NR (Figure 4d–g). Meanwhile, the SIC effect also changes functional groups in NR, where the ethyl ($-CH_2CH_3$), methylene ($-CH_2$), and amide (−CONH−) groups are greatly reduced (Figure 4a). The reduction of these electron-donor groups at the surface region leads to the strain-induced shift in the triboelectric series. X-ray photoelectron spectroscopy (XPS) has also been employed to verify the change in the surface functional groups of NR. Here, the decrease in the ethyl ($-CH_2CH_3$) group and the increase in the −CH═C− group near the surface region can both be confirmed (see Figure S11 and Table S2), which are in good agreement with the results of ATR-FTIR. Noting that the possible influence of material transfer may also lead to a change in electrification performance, we have further studied the material transfer during the contact, as can be seen in Figures S12–S15 and Note 2 in the Supporting Information. A detailed diagram of the reversed electron transfer process (see Figure 2b) that happened on the interface of stretched NR is elaborated in Figure 4h and Figure S16 and Note 3 in the Supporting Information.

In the above studies, we have confirmed that the rearrangement of molecular orientation induced by SIC can induce a shift in polarity in the triboelectric series for NR. On the other hand, the movement ability of the Ecoflex molecular chain decreases at low temperature and a crystallization effect is more likely to occur. Hence, we performed a differential scanning thermal analysis (DSC) to study the low-temperature crystallization of Ecoflex, as shown in Figure 5a. The crystallization peak of Ecoflex appeared at −48 °C, and by integration of the peak area, the melting enthalpy of crystallization was found to be ΔH_{fusion} = 31.17 J g^{-1}. In this case, we selected a temperature of −50 °C as the experimental condition to study the contact electrification of Ecoflex. The experimental results (absolute charge density) of Ecoflex contacting with different materials at both −50 and 20 °C are shown in Figure 5b and Figure S17. The saturated charge

https://doi.org/10.1021/acs.nanolett.2c00767
Nano Lett. XXXX, XXX, XXX−XXX

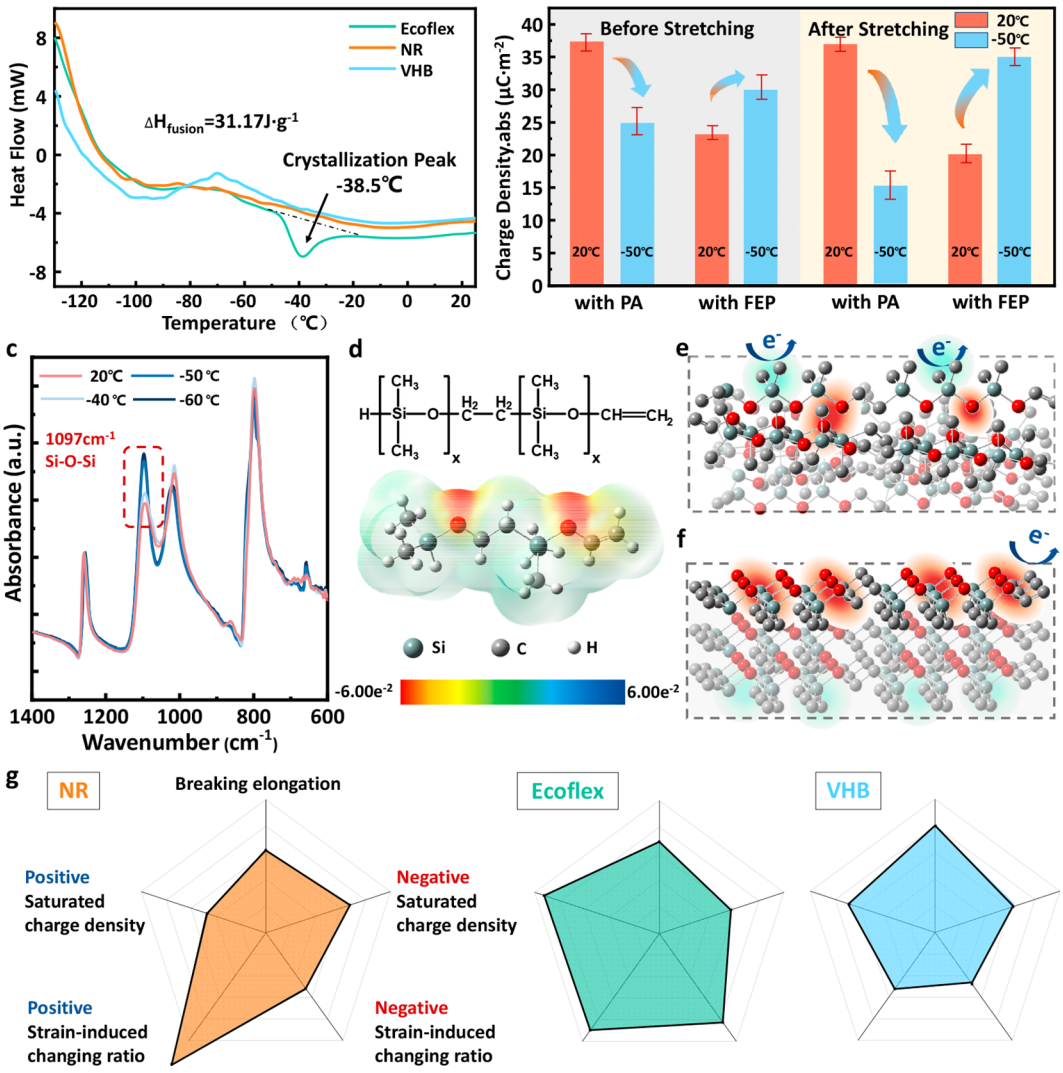

Figure 5. (a) Results of DSC in the range from −130 to 25 °C of Ecoflex, VHB, and NR. (b) Saturated charge densities (absolute values) of Ecoflex at different temperatures on contacting with PA and FEP. The stretching ratio is 400%. (c) Molecular structure changes of Ecoflex at different temperatures as given by ATR-FTIR spectra. (d) Electrostatic potential maps of Ecoflex. (e, f) Schematic models illustrating the corresponding structures of the NR before and after stretching. (g) Comparison of advantages and disadvantages of NR, Ecoflex, and VHB, where the NR shows a significant shift in the triboelectric series, Ecoflex has the highest electrification stability, and VHB maintains the highest breaking elongation. Here, a saturated charge density of 40 μC m^{-2} is taken as the reference value, and the changing ratio means the saturated charge density stretched to 400% divided by the saturated charge density before stretching.

density of Ecoflex and PA decreases at low temperature, while that of Ecoflex and FEP increases, suggesting that the electrification polarity of Ecoflex after crystallization moves to positive direction in the triboelectric series. Moreover, this shift in triboelectric series is more obvious when strain is applied to the Ecoflex film (see Figure 5b), which proves that both stretching and low temperature can promote the crystallization of Ecoflex film. The ATR-FTIR spectra of Ecoflex at −40, −50, and −60 °C have been measured, as shown Figure 5c. With a decrease in temperature, the stretching vibration peak of Si−O at 1097 cm^{-1} gradually increases, suggesting that the number of Si−O bonds increases in the surface region. The strain-enhanced crystallization of silicon rubber at low temperature has also been reported in previous studies on the basis of synchrotron radiation wide-angle X-ray diffraction,[51−53] which can support our explanation for the results in Figure 5b. In order to study the potential distribution of the molecular chain, a DFT calculation was also carried out for the elements on the Ecoflex molecular chain. The electrostatic potential diagram of the structural element is shown in Figure 5d, where the blue and red areas in the figure correspond to electron-poor areas and electron-rich areas, respectively. The results show that the O atom is at the lowest point of the electrostatic potential among all of the elements. In combination with the analysis results of the ATR-FTIR spectrum, the crystallization of the molecular chain at low temperature causes more Si−O bonds to accumulate on the surface region and further enhances the electron-donating capability of Ecoflex. Hence, different from the crystallization of NR, the combined effect of temperature and strain shifts the polarity of Ecoflex to a positive direction in the triboelectric series (Figure 5e,f). It is important to note that, since the shift of polarity under different strains and temperatures has been ignored, it is hard to anticipate the change in the output signal of stretchable TENG, since the charge density can be increased for contacts with one material and be decreased with another.

https://doi.org/10.1021/acs.nanolett.2c00767
Nano Lett. XXXX, XXX, XXX−XXX

We have proposed a modified approach to evaluate the merit of elastic TENG, as can be seen in Figure 5g and Figure S18, Table S3, and Note 4.

In this work, we have selected three types of commonly used elastomers for elastic TENGs and studied their tribo-electrification properties under different strains. The results show that, in addition to the change in effective contact area, crystallization due to strain and a temperature change can also induce a shift in the triboelectric series. The strain-induced crystallization of a molecular chain can generate significant and ordered changes in molecular orientation, which can induce a shift in the triboelectric series or even polarity reversal. This effect can be well explained on the basis of surface electron cloud density. That is, a great change in molecular orientation results in the rearrangement of surface functional groups, which leads to a change in surface electron cloud density and finally shifts the polarity of materials in the triboelectric series. It is also necessary to note that the ordinary extension of a molecular chain, which may only lead to disordered changes, cannot generate a shift in the electrification polarity. More interestingly, the silicone rubber (Ecoflex), the performance of which exhibits little change under different strains at room temperature, can also show a strain-induced shift in the triboelectric series at −50 °C, which can be a good guidance for research on a low-temperature TENG since a lithium-ion battery cannot work effectively at low temperature. This study can help to elucidate the contribution of the molecular spatial orientation of an elastomer to its macroscopic electrical properties, which can further promote the study of stretchable TENGs as energy harvesters or active sensors for wearable electronics.

■ ASSOCIATED CONTENT

Supporting Information

The Supporting Information is available free of charge at https://pubs.acs.org/doi/10.1021/acs.nanolett.2c00767.

Details on materials and methods, detailed explanations and additional figures giving XRD, AFM, XPS, EDS, FTIR, and SEM data (PDF)

Deformation and polarity reversal (MP4)

■ AUTHOR INFORMATION

Corresponding Authors

Xiangyu Chen − *CAS Center for Excellence in Nanoscience, Beijing Institute of Nanoenergy and Nanosystems, Chinese Academy of Sciences, 100083 Beijing, People's Republic of China; School of Nanoscience and Technology, University of Chinese Academy of Sciences, 100049 Beijing, People's Republic of China;* orcid.org/0000-0002-0711-0275; Email: chenxiangyu@binn.cas.cn

Zhong Lin Wang − *CAS Center for Excellence in Nanoscience, Beijing Institute of Nanoenergy and Nanosystems, Chinese Academy of Sciences, 100083 Beijing, People's Republic of China; School of Nanoscience and Technology, University of Chinese Academy of Sciences, 100049 Beijing, People's Republic of China; School of Materials Science and Engineering, Georgia Institute of Technology, Atlanta, Georgia 30332-0245, United States;* orcid.org/0000-0002-5530-0380; Email: zhong.wang@mse.gatech.edu

Authors

Zhaoqi Liu − *CAS Center for Excellence in Nanoscience, Beijing Institute of Nanoenergy and Nanosystems, Chinese Academy of Sciences, 100083 Beijing, People's Republic of China; School of Nanoscience and Technology, University of Chinese Academy of Sciences, 100049 Beijing, People's Republic of China*

Shuyao Li − *CAS Center for Excellence in Nanoscience, Beijing Institute of Nanoenergy and Nanosystems, Chinese Academy of Sciences, 100083 Beijing, People's Republic of China; School of Nanoscience and Technology, University of Chinese Academy of Sciences, 100049 Beijing, People's Republic of China;* orcid.org/0000-0003-2156-4684

Shiquan Lin − *CAS Center for Excellence in Nanoscience, Beijing Institute of Nanoenergy and Nanosystems, Chinese Academy of Sciences, 100083 Beijing, People's Republic of China; School of Nanoscience and Technology, University of Chinese Academy of Sciences, 100049 Beijing, People's Republic of China*

Yuxiang Shi − *CAS Center for Excellence in Nanoscience, Beijing Institute of Nanoenergy and Nanosystems, Chinese Academy of Sciences, 100083 Beijing, People's Republic of China; School of Nanoscience and Technology, University of Chinese Academy of Sciences, 100049 Beijing, People's Republic of China;* orcid.org/0000-0001-5112-4159

Peng Yang − *CAS Center for Excellence in Nanoscience, Beijing Institute of Nanoenergy and Nanosystems, Chinese Academy of Sciences, 100083 Beijing, People's Republic of China; School of Nanoscience and Technology, University of Chinese Academy of Sciences, 100049 Beijing, People's Republic of China*

Complete contact information is available at: https://pubs.acs.org/10.1021/acs.nanolett.2c00767

Author Contributions

X.C. and Z.L.W. conceived the idea and supervised the experiment. Z.L. and X.C. prepared the manuscript. Z.L. and S. Li designed the structure of the device. Z.L. performed the data measurements. S.Lin helped with the AFM. P.Y. offered assistance with the experiments. All of the authors discussed the results and commented on the manuscript.

Notes

The authors declare no competing financial interest.

■ ACKNOWLEDGMENTS

This work was supported by the National Key R&D Project from the Ministry of Science and Technology (2021YFA1201601), the National Natural Science Foundation of China (Grant No. 62174014), the Beijing Nova program (Z201100006820063) , and the Youth Innovation Promotion Association CAS (2021165). We thank Professor Dan Yang (Beijing University of Chemical Technology) for helping with the fabrication of the NR film.

■ REFERENCES

(1) Matsuhisa, N.; Niu, S.; O'Neill, S. J. K.; Kang, J.; Ochiai, Y.; Katsumata, T.; Wu, H.-C.; Ashizawa, M.; Wang, G.-J. N.; Zhong, D.; et al. High-frequency and intrinsically stretchable polymer diodes. *Nature* **2021**, *600* (7888), 246−252.

(2) Yang, Q.; Wei, T.; Yin, R. T.; Wu, M.; Xu, Y.; Koo, J.; Choi, Y. S.; Xie, Z.; Chen, S. W.; Kandela, I.; et al. Photocurable bioresorbable adhesives as functional interfaces between flexible bioelectronic

devices and soft biological tissues. *Nat. Mater.* **2021**, *20* (11), 1559−1570.
(3) Chung, H. U.; Rwei, A. Y.; Hourlier-Fargette, A.; Xu, S.; Lee, K.; Dunne, E. C.; Xie, Z.; Liu, C.; Carlini, A.; Kim, D. H.; et al. Skin-interfaced biosensors for advanced wireless physiological monitoring in neonatal and pediatric intensive-care units. *Nat. Med.* **2020**, *26* (3), 418−429.
(4) Huang, Y.; Zhong, M.; Huang, Y.; Zhu, M.; Pei, Z.; Wang, Z.; Xue, Q.; Xie, X.; Zhi, C. A self-healable and highly stretchable supercapacitor based on a dual crosslinked polyelectrolyte. *Nat. Commun.* **2015**, *6*, 10310.
(5) Chen, X.; Wu, Y.; Shao, J.; Jiang, T.; Yu, A.; Xu, L.; Wang, Z. L. On-Skin Triboelectric Nanogenerator and Self-Powered Sensor with Ultrathin Thickness and High Stretchability. *Small* **2017**, *13* (47), 1702929.
(6) Tao, X.; Li, S.; Shi, Y.; Wang, X.; Tian, J.; Liu, Z.; Yang, P.; Chen, X.; Wang, Z. L. Triboelectric Polymer with High Thermal Charge Stability for Harvesting Energy from 200 °C Flowing Air. *Adv. Funct. Mater.* **2021**, *31* (49), 2106082.
(7) Tat, T.; Libanori, A.; Au, C.; Yau, A.; Chen, J. Advances in triboelectric nanogenerators for biomedical sensing. *Biosens. Bioelectron.* **2021**, *171*, 112714.
(8) Wang, H.; Cheng, J.; Wang, Z.; Ji, L.; Wang, Z. L. Triboelectric nanogenerators for human-health care. *Sci. Bull.* **2021**, *66* (5), 490−511.
(9) Wang, J.; Cai, G.; Li, S.; Gao, D.; Xiong, J.; Lee, P. S. Printable Superelastic Conductors with Extreme Stretchability and Robust Cycling Endurance Enabled by Liquid-Metal Particles. *Adv. Mater.* **2018**, *30* (16), 1706157.
(10) Cai, G.; Wang, J.; Qian, K.; Chen, J.; Li, S.; Lee, P. S. Extremely Stretchable Strain Sensors Based on Conductive Self-Healing Dynamic Cross-Links Hydrogels for Human-Motion Detection. *Adv. Sci.* **2017**, *4* (2), 1600190.
(11) Tee, B. C. K.; Wang, C.; Allen, R.; Bao, Z. An electrically and mechanically self-healing composite with pressure- and flexion-sensitive properties for electronic skin applications. *Nat. Nanotechnol.* **2012**, *7* (12), 825−832.
(12) Wu, C.; Wang, X.; Lin, L.; Guo, H.; Wang, Z. L. Paper-Based Triboelectric Nanogenerators Made of Stretchable Interlocking Kirigami Patterns. *ACS Nano* **2016**, *10* (4), 4652−4659.
(13) Xia, X.; Chen, J.; Liu, G.; Javed, M. S.; Wang, X.; Hu, C. Aligning graphene sheets in PDMS for improving output performance of triboelectric nanogenerator. *Carbon* **2017**, *111*, 569−576.
(14) Cai, Y.-W.; Zhang, X.-N.; Wang, G.-G.; Li, G.-Z.; Zhao, D.-Q.; Sun, N.; Li, F.; Zhang, H.-Y.; Han, J.-C.; Yang, Y. A flexible ultra-sensitive triboelectric tactile sensor of wrinkled PDMS/MXene composite films for E-skin. *Nano Energy* **2021**, *81*, 105663.
(15) Yang, D.; Ni, Y.; Kong, X.; Li, S.; Chen, X.; Zhang, L.; Wang, Z. L. Self-Healing and Elastic Triboelectric Nanogenerators for Muscle Motion Monitoring and Photothermal Treatment. *ACS Nano* **2021**, *15* (9), 14653−14661.
(16) Lee, Y.; Cha, S. H.; Kim, Y.-W.; Choi, D.; Sun, J.-Y. Transparent and attachable ionic communicators based on self-cleanable triboelectric nanogenerators. *Nat. Commun.* **2018**, *9* (1), 1804.
(17) Pu, X.; Liu, M.; Chen, X.; Sun, J.; Du, C.; Zhang, Y.; Zhai, J.; Hu, W.; Wang, Z. L. Ultrastretchable, transparent triboelectric nanogenerator as electronic skin for biomechanical energy harvesting and tactile sensing. *Sci. Adv.* **2017**, *3* (5), e1700015.
(18) Parida, K.; Thangavel, G.; Cai, G.; Zhou, X.; Park, S.; Xiong, J.; Lee, P. S. Extremely stretchable and self-healing conductor based on thermoplastic elastomer for all-three-dimensional printed triboelectric nanogenerator. *Nat. Commun.* **2019**, *10* (1), 2158.
(19) Lacks, D. J.; Shinbrot, T. Long-standing and unresolved issues in triboelectric charging. *Nat. Rev. Chem.* **2019**, *3* (8), 465−476.
(20) Kaponig, M.; Mölleken, A.; Nienhaus, H.; Möller, R. Dynamics of contact electrification. *Sci. Adv.* **2021**, *7* (22), eabg7595.
(21) Wen, Z.; Yang, Y.; Sun, N.; Li, G.; Liu, Y.; Chen, C.; Shi, J.; Xie, L.; Jiang, H.; Bao, D. A Wrinkled PEDOT:PSS Film Based Stretchable and Transparent Triboelectric Nanogenerator for Wearable Energy Harvesters and Active Motion Sensors. *Adv. Funct. Mater.* **2018**, *28* (37), 1803684.
(22) Yang, Y.; Han, J.; Huang, J.; Sun, J.; Wang, Z. L.; Seo, S.; Sun, Q. Stretchable Energy-Harvesting Tactile Interactive Interface with Liquid-Metal-Nanoparticle-Based Electrodes. *Adv. Funct. Mater.* **2020**, *30* (29), 1909652.
(23) Sun, L.; Chen, S.; Guo, Y.; Song, J.; Zhang, L.; Xiao, L.; Guan, Q.; You, Z. Ionogel-based, highly stretchable, transparent, durable triboelectric nanogenerators for energy harvesting and motion sensing over a wide temperature range. *Nano Energy* **2019**, *63*, 103847.
(24) Li, S.; Fan, Y.; Chen, H.; Nie, J.; Liang, Y.; Tao, X.; Zhang, J.; Chen, X.; Fu, E.; Wang, Z. L. Manipulating the triboelectric surface charge density of polymers by low-energy helium ion irradiation/implantation. *Energy Environ. Sci.* **2020**, *13* (3), 896−907.
(25) Li, S.; Nie, J.; Shi, Y.; Tao, X.; Wang, F.; Tian, J.; Lin, S.; Chen, X.; Wang, Z. L. Contributions of Different Functional Groups to Contact Electrification of Polymers. *Adv. Mater.* **2020**, *32* (25), 2001307.
(26) Tao, X.; Nie, J.; Li, S.; Shi, Y.; Lin, S.; Chen, X.; Wang, Z. L. Effect of Photo-Excitation on Contact Electrification at Liquid−Solid Interface. *ACS Nano* **2021**, *15* (6), 10609−10617.
(27) Wang, F.; Yang, P.; Tao, X.; Shi, Y.; Li, S.; Liu, Z.; Chen, X.; Wang, Z. L. Study of Contact Electrification at Liquid-Gas Interface. *ACS Nano* **2021**, *15* (11), 18206−18213.
(28) Lapcinskis, L.; Linarts, A.; Malnieks, K.; Kim, H.; Rubenis, K.; Pudzs, K.; Smits, K.; Kovalovs, A.; Kalnins, K.; Tamm, A.; Jeong, C. K.; Sutka, A.; et al. Triboelectrification of nanocomposites using identical polymer matrixes with different concentrations of nanoparticle fillers. *Journal of Materials Chemistry A* **2021**, *9* (14), 8984−8990.
(29) Sutka, A.; Malnieks, K.; Lapcinskis, L.; Timusk, M.; Kalnins, K.; Kovalovs, A.; Bitenieks, J.; Knite, M.; Stevens, D.; Grunlan, J. Contact electrification between identical polymers as the basis for triboelectric/flexoelectric materials. *Phys. Chem. Chem. Phys.* **2020**, *22* (23), 13299−13305.
(30) Lee, S.; Lee, Y.; Kim, D.; Yang, Y.; Lin, L.; Lin, Z. H.; Hwang, W.; Wang, Z. L. Triboelectric nanogenerator for harvesting pendulum oscillation energy. *Nano Energy* **2013**, *2* (6), 1113−1120.
(31) Sutka, A.; Malnieks, K.; Lapcinskis, L.; Kaufelde, P.; Linarts, A.; Berzina, A.; Zabels, R.; Jurkans, V.; Gornevs, I.; Blums, J.; Knite, M.; et al. The role of intermolecular forces in contact electrification on polymer surfaces and triboelectric nanogenerators. *Energy Environ. Sci.* **2019**, *12* (8), 2417−2421.
(32) Xu, C.; Zhang, B.; Wang, A. C.; Zou, H.; Liu, G.; Ding, W.; Wu, C.; Ma, M.; Feng, P.; Lin, Z.; et al. Contact-Electrification between Two Identical Materials: Curvature Effect. *ACS Nano* **2019**, *13* (2), 2034−2041.
(33) Wang, Z.; Sun, B.; Lu, X.; Wang, C.; Su, Z. Molecular Orientation in Individual Electrospun Nanofibers Studied by Polarized AFM−IR. *Macromolecules* **2019**, *52* (24), 9639−9645.
(34) Wang, R.; Fang, S.; Xiao, Y.; Gao, E.; Jiang, N.; Li, Y.; Mou, L.; Shen, Y.; Zhao, W.; Li, S.; et al. Torsional refrigeration by twisted, coiled, and supercoiled fibers. *Science* **2019**, *366* (6462), 216−221.
(35) Sow, M.; Lacks, D. J.; Sankaran, R. M. Dependence of contact electrification on the magnitude of strain in polymeric materials. *J. Appl. Phys.* **2012**, *112* (8), 084909.
(36) Parida, K.; Bhavanasi, V.; Kumar, V.; Wang, J.; Lee, P. S. Fast charging self-powered electric double layer capacitor. *J. Power Sources* **2017**, *342*, 70−78.
(37) Sow, M.; Widenor, R.; Kumar, A.; Lee, S. W.; Lacks, D. J.; Sankaran, R. M. Strain-induced reversal of charge transfer in contact electrification. *Angew. Chem., Int. Ed. Engl.* **2012**, *51* (11), 2695−2697.
(38) Horn, R. G.; Smith, D. T.; Grabbe, A. Contact electrification induced by monolayer modification of a surface and relation to acid−base interactions. *Nature* **1993**, *366* (6454), 442−443.
(39) Niu, S.; Liu, Y.; Wang, S.; Lin, L.; Zhou, Y. S.; Hu, Y.; Wang, Z. L. Theoretical Investigation and Structural Optimization of Single-

https://doi.org/10.1021/acs.nanolett.2c00767
Nano Lett. XXXX, XXX, XXX−XXX

Electrode Triboelectric Nanogenerators. *Adv. Funct. Mater.* **2014**, *24* (22), 3332−3340.
(40) Bunriw, W.; Harnchana, V.; Chanthad, C.; Huynh, V. N. Natural Rubber-TiO2 Nanocomposite Film for Triboelectric Nanogenerator Application. *Polymers* **2021**, *13* (13), 2213.
(41) Salauddin, M.; Rana, S. M. S.; Sharifuzzaman, M.; Rahman, M. T.; Park, C.; Cho, H.; Maharjan, P.; Bhatta, T.; Park, J. Y. A Novel MXene/Ecoflex Nanocomposite-Coated Fabric as a Highly Negative and Stable Friction Layer for High-Output Triboelectric Nanogenerators. *Adv. Energy Mater.* **2021**, *11* (1), 2002832.
(42) Xu, Z.; Zhou, F.; Yan, H.; Gao, G.; Li, H.; Li, R.; Chen, T. Antifreezing organohydrogel triboelectric nanogenerator toward highly efficient and flexible human-machine interaction at − 30 °C. *Nano Energy* **2021**, *90*, 106614.
(43) Zou, H.; Guo, L.; Xue, H.; Zhang, Y.; Shen, X.; Liu, X.; Wang, P.; He, X.; Dai, G.; Jiang, P.; et al. Quantifying and understanding the triboelectric series of inorganic non-metallic materials. *Nat. Commun.* **2020**, *11* (1), 2093.
(44) Xu, C.; Zi, Y.; Wang, A. C.; Zou, H.; Dai, Y.; He, X.; Wang, P.; Wang, Y.-C.; Feng, P.; Li, D.; et al. On the Electron-Transfer Mechanism in the Contact-Electrification Effect. *Adv. Mater.* **2018**, *30* (15), 1706790.
(45) Lin, S.; Xu, L.; Zhu, L.; Chen, X.; Wang, Z. L. Electron Transfer in Nanoscale Contact Electrification: Photon Excitation Effect. *Adv. Mater.* **2019**, *31* (27), 1901418.
(46) Wang, Z. L.; Wang, A. C. On the origin of contact-electrification. *Mater. Today* **2019**, *30*, 34−51.
(47) Zhang, X.; Sun, S.; Ning, N.; Yan, S.; Wu, X.; Lu, Y.; Zhang, L. Visualization and Quantification of the Microstructure Evolution of Isoprene Rubber during Uniaxial Stretching Using AFM Nanomechanical Mapping. *Macromolecules* **2020**, *53* (8), 3082−3089.
(48) Amram, B.; Bokobza, L.; Queslel, J. P.; Monnerie, L. Fourier-transform infra-red dichroism study of molecular orientation in synthetic high cis-1,4-polyisoprene and in natural rubber. *Polymer* **1986**, *27* (6), 877−882.
(49) Healey, A. M.; Hendra, P. J.; West, Y. D. A Fourier-transform Raman study of the strain-induced crystallization and cold crystallization of natural rubber. *Polymer* **1996**, *37* (18), 4009−4024.
(50) Toki, S.; Hsiao, B. S. Nature of Strain-Induced Structures in Natural and Synthetic Rubbers under Stretching. *Macromolecules* **2003**, *36* (16), 5915−5917.
(51) Chen, P.; Zhao, J.; Lin, Y.; Chang, J.; Meng, L.; Wang, D.; Chen, W.; Chen, L.; Li, L. In situ characterization of strain-induced crystallization of natural rubber by synchrotron radiation wide-angle X-ray diffraction: construction of a crystal network at low temperatures. *Soft Matter* **2019**, *15* (4), 734−743.
(52) Zhao, J.; Chen, P.; Lin, Y.; Chang, J.; Lu, A.; Chen, W.; Meng, L.; Wang, D.; Li, L. Stretch-Induced Crystallization and Phase Transitions of Poly(dimethylsiloxane) at Low Temperatures: An in Situ Synchrotron Radiation Wide-Angle X-ray Scattering Study. *Macromolecules* **2018**, *51* (21), 8424−8434.
(53) Zhao, J.; Feng, S.; Zhang, W.; Chen, W.; Sheng, J.; Yu, W.; Li, L. Strain Rate Dependence of Stretch-Induced Crystallization and Crystal Transition of Poly(dimethylsiloxane). *Macromolecules* **2021**, *54* (19), 9204−9216.

https://doi.org/10.1021/acs.nanolett.2c00767
Nano Lett. XXXX, XXX, XXX−XXX